Mater. Res. Soc. Symp. Proc. Vol. 1659 © 2014 Materials Research Society
DOI: 10.1557/opl.2014.211

Ultraviolet Photodetector Fabricated from 3D WO_3 Nanowires/Reduced Graphene Oxide Composite Material

Dali Shao,[1] MingpengYu,[2,3] Jie Lian,[2] and Shayla Sawyer[1]
[1]Department of Electrical, Computer, and Systems Engineering, Rensselaer Polytechnic Institute, Troy, NY 12180, USA
[2]Department of Mechanical, Aerospace & Nuclear Engineering, Rensselaer Polytechnic Institute, Troy, NY 12180, USA
[3] Department of Chemistry, Laboratory of Bio-organic Phosphorus, Tsinghua University, Beijing 100084, China.

ABSTRACT

An Ultraviolet (UV) photodetector with high responsivity and relative fast response speed was fabricated from three dimensional WO_3 nanowires/reduced graphene oxide (3D WO_3 NWs/RGO) composite materials. The 3D WO_3 NDs/GN composite was synthesized using a facile three-step synthesis. First, the Na_2WO_4/Graphene Oxide (GO) precursor was synthesized by homogeneous precipitation. Second, the Na_2WO_4/GO precursor was transformed into H_2WO_4/GO composites by acidification. Finally, the H_2WO_4/GO composites were reduced to 3D WO_3 NWs/RGO via hydrothermal reduction process. A maximum photoresponsivity of 4.2 A/W at 374 nm was observed under 20 V bias. The UV photodetector showed relative fast transient response, which is at least 2 orders of magnitude faster than UV photodetectors fabricated from WO_3 nanowires. The good photoresponsivity and fast transient response are attributed to improved carrier transport and collection efficiency through graphene.

INTRODUCTION

Ultraviolet (UV) photodetectors have been investigated for various commercial and military applications, such as secure space-to-space communications, pollution monitoring, water sterilization, flame sensing and early missile plume detection [1]. To date, many different wide bandgap semiconductors such as GaN, ZnO, Si_3N_4, and In_2O_3 nanostructures have been extensively studied for UV photodetector applications [2-7]. However, only a few work reported tungsten oxide (WO_3) nanomaterial for UV radiation detection [8-10].

In this work, an UV photodetector was fabricated from WO_3 nanowires (NWs)/reduced graphene oxide (RGO) composite material. The WO_3 NWs/RGO composite material was synthesized using a facile three-step synthesis procedure. First, the Na_2WO_4/GO precursor was synthesized by homogeneous precipitation. Second, the Na_2WO_4/GO precursor was transformed into H_2WO_4/GO composites by acidification. Finally, the H_2WO_4/GO composites were reduced to 3D WO_3 NWs/RGO via hydrothermal reduction process. The UV photodetector showed fast transient response (on the order of milliseconds) and high responsivity (4.2 A/W), which are attributed to improved carrier transport and collection efficiency through graphene.

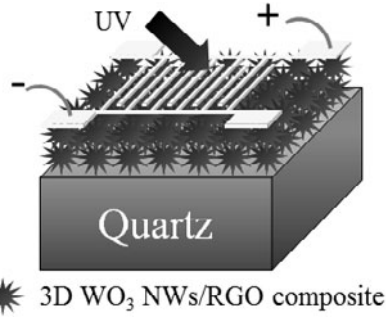

Figure 1. Schematic illustration of the UV photodetector fabricated from the 3D WO_3 NWs/RGO composite material

EXPERIMENTAL DETAILS

The 3D WO_3 NWs were grown using an *in situ* hydrothermal process. In this process, 0.85 g $Na_2WO_4 \cdot 2H_2O$ and 0.15 g NaCl were dissolved in deionized water and kept stirring for 6 hours. Then, 2M hydrochloric acid solution was added dropwise to the above solution until the pH of the solution was adjusted to approximate 2.0. After that, the solution was transferred into a Teflon-lined stainless steel autoclave (Parr, 4744) and heated to 190 °C. After 20 hours hydrothermal treatment, the autoclave was cooled down to room temperature naturally. The precipitate was centrifuged, washed with ethanol and deionized water 6 times and finally dried at 60 °C under vacuum for further characterization.

The growth mechanism of the 3D WO_3 NWs/Graphene nanocomposite structure is presented as the following. First, due to the oxygen-containing functional groups on the GO sheets, the GO surface can easily absorb Na^{2+} ions in aqueous solution through electrostatic interactions, and then interact with WO_4^{2-} to form Na_2WO_4 on the GO sheets [10]. Second, a large amount of H_2WO_4 was formed and attached to the surface of GO after the addition of HCl solution through acidification process. Third, H_2WO_4 was decomposed into WO_3 crystal nucleus under the hydrothermal environment, which triggered the nucleation and preferential growth along c-axes in the presence of NaCl. The oxygen-containing functional groups located at the surface of GO sheet act as anchor sites and enabled the subsequent formation of small WO_3 NWs on the surface. At the same time, hydrothermal reduction at high temperature was reported to be an effective route to restore the sp^2-hybridized network. Thus, the increased temperature and pressure led to the rupture of oxygen-containing groups not involved in the reaction. As a result, GO was simultaneously reduced to RGO, accompanied with the growth of WO_3 NWs during the hydrothermal reaction.

The UV photodetector was fabricated by deposition of the 3D WO_3 NWs on quartz substrate via spin casting deposition method. Then, interdigitated Al contacts with thickness of 250 nm were deposited on the top using electron beam evaporator. Finally, the photodetector was packaged and wire bonded using Epo-Tek H20E conductive epoxy. The schematic illustration of the UV photodetector is shown in figure 1.

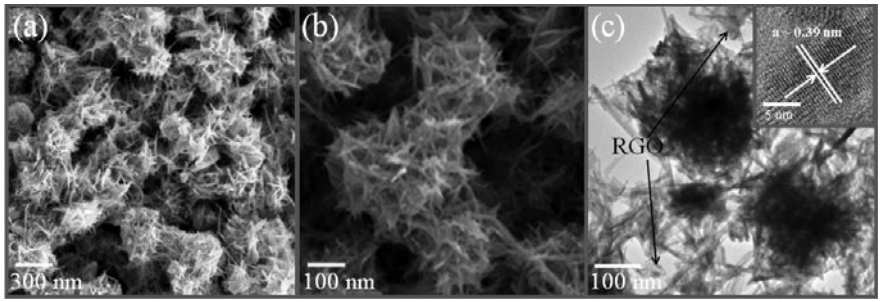

Figure 2. SEM images of the 3D WO_3 NWs/RGO composite with (a) medium magnification and (b) high magnification. (c) TEM image and HRTEM (inset) image of the 3D WO_3 NWs/RGO

The morphology and microstructure of the 3D WO_3 NWs structure was characterized by a dual beam scanning electron microscopy (SEM, Carl Zeiss Ultra 1540). The crystal structure of the 3D WO_3 NWs was confirmed using a high resolution transmission electron microscopy (HRTEM, JEOL 2011). The X-ray diffraction (XRD, PANalytical) patterns was measured at room temperature with Cu Kα radiation (wavelength = 1.54 Å). The chemical state of the WO_3 NWs was characterized by X-ray photoelectron spectroscopy (XPS, PHI 5000 Versa Probe). The typical I-V characteristics and photoresponsivity of the photodetector fabricated from the 3D WO_3 NWs were measured using a HP4155B semiconductor parameter analyzer and a Shimadzu UV-Vis 2550 in connection with a Newport 1928-C optical power meter, respectively.

DISCUSSION

The SEM images of the 3D WO_3 NWs/RGO composite are shown in figure 2a and b. The TEM image of the 3D WO_3 NWs/RGO is shown in figure 2c. It can be seen clearly from figure 2b that the 3D WO_3 NWs have high surface to volume ratio, which is favorable for photodetector and gas sensing applications. The HRTEM image of the 3D WO_3 NWs/RGO is shown in the inset of figure 2c, from which the space of the lattice fringes is determined to be 0.39 nm, corresponding to the (001) plane of the WO_3 hexagonal cell. This indicates that the 3D WO_3 NWs were grown along the c-axis direction [10].

Figure 3a shows the XRD patterns of the 3D WO_3 NWs/RGO. All the peaks can be well indexed to hexagonal structure of WO_3 (JCPDS 75-2187) with the space group P6/mmm. Figure 3b shows the W 4f core-level spectrum for the 3D WO_3 NWs measured by XPS. Two major peaks for W $4f_{7/2}$ and W $4f_{5/2}$ were observed at 35.6 and 37.8eV, respectively. These results are consistent with previous report, indicating stoichiometric WO_3 in the NWs structure [11].

The typical I-V characteristics of the photodetector were measured under dark environment and under 335 nm UV illuminations with the light intensity of 31.65 mW/cm^2, as shown in figure 4a. The photocurrent to dark current ratio is around 27 at 20 V. The photoconductivity mechanism of the WO_3 NWs/RGO is attributed to surface oxygen adsorption and desorption process, which has been discussed in details in our previous works [10]. The transient response of the photodetector is shown in figure 4b, which was measured by turning on and off a UV LED

with peak wavelength at 335 nm. The rise time and fall time of the photodetector were measured to be ~46 ms and ~22 ms, respectively. This is at least 2 orders of magnitude faster than UV photodetectors fabricated from WO_3 nanowires [8, 9]. The fast transient response originates from improved carrier transport and collection efficiency through RGO [10]. Briefly, the electron affinity of the molecule WO_3 is lower than the work function of the RGO [10]. Therefore, when WO_3 is in contact with the RGO, it is energetically favorable for the photogenerated electron to transfer from the conduction band of WO_3 to the RGO side. However, this will suppress the oxygen adsorption and desorption process and reduce the internal gain RGO have high carrier mobility, less accumulation of the electrons on RGO side is expected. When UV illumination is turned off, the excess electrons in the RGO side transfer to the WO_3 side for recombination with holes, which is a very fast process [10]. Thus, the carrier transport efficiency can be effectively improved, leading to a fast rise and decay of the photocurrent.

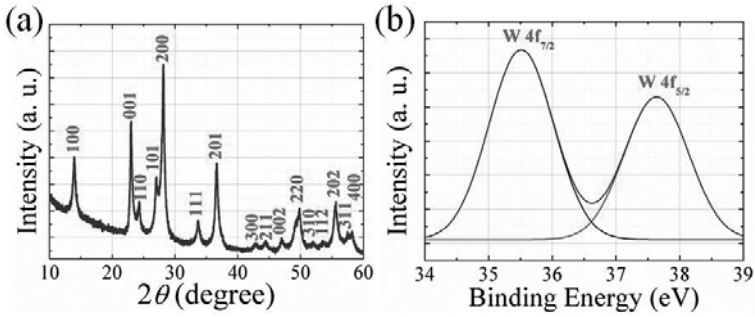

Figure 3. (a) XRD pattern and (b) W 4f peaks of the 3D WO_3 nanoshale structure.

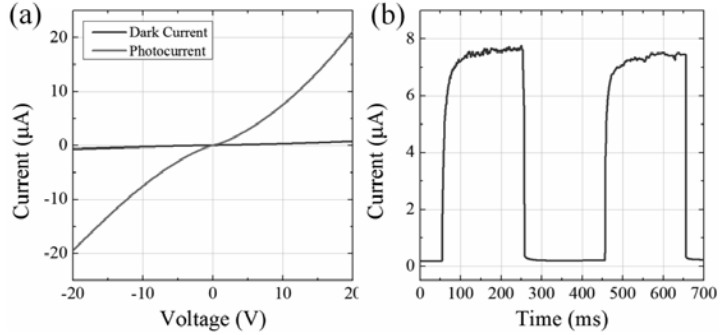

Figure 4. (a) Typical I-V characteristics and (b) transient response of the UV photodetector fabricated from the 3D WO_3 NWs/RGO composite material.

The photoresponsivity of the photodetector, defined as photocurrent per unit of incident optical power, is shown in figure 5. A maximum photoresponsivity of 4.2 A/W at 374 nm was observed under 20 V, which is more than 20 times higher than those of commercial GaN or SiC photodetectors (< 0.2 A/W) [12]. The inset of figure 5 shows the external quantum efficiency (EQE) of the photodetector calculated using the equation: EQE=R×hν/q, where hν is the energy of the incident photon in electronvolts, q is the electron charge and R is the photoresponsivity of the UV photodetector. The maximum EQE is calculated to be 1442% at 374 nm. Such a high EQE of the UV photodetector is attributed to both carrier transport and collection efficiency by graphene and the internal gain that introduced by the oxygen adsorption/desorption process at the surface of 3D WO_3 NWs structure [10]. It is worth to mention that the incorporation of RGO can suppress the oxygen adsorption/desorption process as many electrons are transported through graphene rather than WO_3. This can improve the transient response but may reduce the gain of the pure WO_3 material. However, the improvement of carrier transport and collection efficiency by graphene may outweigh the reduced gain effect and it is possible to achieve both improved transient response and photoresponsivity.

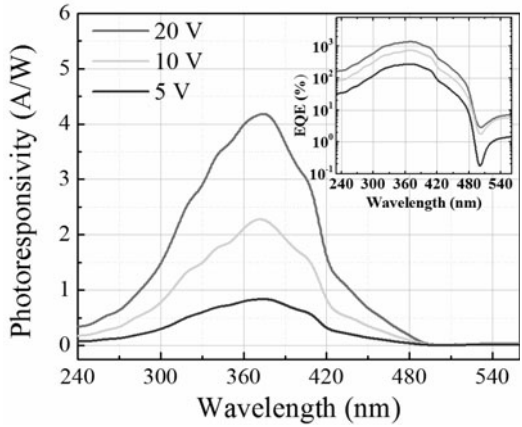

Figure 5. Photoresponsivity spectra of the UV photodetector fabricated from the 3D WO_3 NWs/RGO composite material. Inset: calculated EQE of the UV photodetector.

.

CONCLUSIONS

In conclusion, we synthesized a novel 3D WO_3 NWs/RGO composite material using a facile hydrothermal procedure. An UV photodetector fabricated from the 3D WO_3 NWs/RGO composite material showed a good photoresponsivity (4.2 A/W) and relative fast transient response, which is due to improved carrier transport and collection efficiency through RGO. The good material properties of the 3D WO_3 NWs/RGO demonstrated in this work may open up new

possibilities for using WO_3 for future optoelectronic applications such as photodetectors and optical switches.

ACKNOWLEDGMENTS

The authors gratefully acknowledge support from National Security Technologies through NSF Industry/University Cooperative Research Center Connection One. The authors also acknowledge the National Science Foundation Smart Lighting Engineering Research Center (EEC-0812056) and a NSF career award DMR 1151028.

REFERENCES:

1. T. V. Blank, and Y. A. Gol'dberg, *Semicond.* **37**, 999 (2003).
2. D. Li, X. Sun, H. Song, Z. Li, Y. Chen, H. Jiang, and G. Miao, *Adv. Mater.* **24**, 845 (2012).
3. D. Shao, M. Yu, H. Sun, T. Hu, J. Lian, and S. Sawyer, *Nanoscale* **5**, 3664 (2013).
4. D. Shao, M. Yu, J. Lian, and S. Sawyer, *Appl. Phys. Lett.* **101**, 211103 (2012).
5. D. Shao, M. Yu, J. Lian, and S. Sawyer, *Appl. Phys. Lett.* **102**, 021107 (2013).
6. J. Y. Zhang, Y. X. Chen, T. L. Guo, Z. X. Lin, and T. H. Wang, *Nanotech.* **18**, 325603 (2007).
7. D. Shao, L. Qin and S. Sawyer, *IEEE Photonics J.* **4**, 715 (2012).
8. K. Huang, Q. Zhang, F. Yang and D. He, *Nano Res.* **3**, 281 (2010).
9. L. Li, Y. Zhang, X. Fang, T. Zhai, M. Liao, X. Sun, Y. Koide, Y. Bando, and D. J. Golberg, *Mater. Chem.* **21**, 6525 (2011).
10. D. Shao, M. Yu, J. Lian, and S. Sawyer, *Nanotechnol.* **24**, 295701 (2013).
11. P. R. Bueno, F. M. Pontes, E. R. Leite, L. O. S. Bulhões, P. S. Pizani, P. N. Lisboa-Filho, and W. H. Schreiner, *J. Appl. Phys.* **96**, 2102 (2004).
12. Y. Z. Jin, J. P. Wang, B. Q. Sun, J. C. Blakesley, and N. C. Greenham, *Nano Lett.* **8** 1649 (2008).